Dynamic covalent properties of a novel indolo[3,2-b]carbazole diradical

Article

Accepted Version

It is advisable to refer to the publisher's version if you intend to cite from the work. See Guidance on citing.

To link to this article DOI: http://dx.doi.org/10.1002/chem.202005211

Publisher: Wiley

www.reading.ac.uk/centaur

CentAUR

Central Archive at the University of Reading

Reading's research outputs online

Accepted Article

Authors: Maria Carmen Ruiz Delgado, Irene Badía-Domínguez, Miriam Peña Álvarez, Deliang Wang, Andrés Pérez-Guardiola, Yolanda Vida Pol, Sandra Rodríguez-González, Juan T. López Navarrete, Víctor Hernández Jolín, Juan C. Sancho García, Valentín García Baonza, Rosie Nash, František Hartl, and Hongxiang Li

WILEY-VCH

Dynamic Covalent Properties of a Novel Indolo[3,2-b]carbazole Diradical

Irene Badía Domínguez,[a] Miriam Peña Álvarez,[b]1 Deliang Wang,[c] Andrés Pérez Guardiola,[d] Yolanda Vida, [e,f] Sandra Rodríguez González,[a] Juan T. López Navarrete,[a] Víctor Hernández Jolín,[a] Juan C. Sancho García,[d] Valentín García Baonza,[g] Rosie Nash,[h] František Hartl,[h]* Hongxiang Li,[c]* M. Carmen Ruiz Delgado [a]*

[a] Department of Physical Chemistry, University of Málaga, Campus de Teatinos s/n, 229071, Málaga, Spain.
[b] Centre for Science at Extreme Conditions & School of Physics and Astronomy, University of Edinburgh, Edinburgh EH9 3FD, United Kingdom.
[c] Key Laboratory of Synthetic and Self-assembly Chemistry for Organic Functional Materials, Shanghai Institute of Organic Chemistry, Chinese Academy of Sciences, Shanghai, 200032, China.
[d] Department of Physical Chemistry, University of Alicante, E-03080 Alicante, Spain.
[e] Universidad de Málaga - IBIMA, Dpto. Química Orgánica, Campus de Teatinos s/n, 29071 Málaga, Spain.
[f] Centro Andaluz de Nanomedicina y Biotecnología-BIONAND. Parque Tecnológico de Andalucía, C/ Severo Ochoa, 35, 29590 Campanillas, Málaga, Spain
[g] MALTA-Consolider Team and Instituto de Geociencias IGEO (CSIC-ICM), University Complutense of Madrid, 28040 Madrid, Spain
[h] Department of Chemistry, University of Reading, Whiteknights, Reading RG6 6DX, United Kingdom. E-mail: f.hartl@reading.ac.uk

Abstract

This work describes the synthesis and properties of a dicyanomethylene-susbtituted indolo[3,2-b]carbazole diradical **ICz-CN**. This quinoidal system dimerises almost completely to (**ICz-CN**)$_2$ containing two long C(sp^3)–C(sp^3) σ-bonds between the dicyanomethylene units**.** The minor open-shell **ICz-CN** component in the solid-state mixture was identified with EPR spectroscopy. The cyclic voltammetric and UV-vis spectroelectrochemical data, and comparison with reference monomer **ICz-Br** reveal that the nature of the one-electron oxidation of (**ICz-CN**)$_2$ at ambient temperature and **ICz-CN** at elevated temperature is very similar in all these compounds due to the prevailing localization of their HOMO on the **ICz** backbone. The peculiar cathodic behaviour reflects the co-existence of (**ICz-CN**)$_2$ and **ICz-CN**. The involvement of the dicyanomethylene groups stabilizes the close-lying LUMO and LUMO+1 of both (**ICz-CN**)$_2$ and especially **ICz-CN** compared to **ICz-Br**, resulting in the distinctive cathodic response at low overpotentials. Differently from neutral **ICz-CN**, its radical anion and dianion are remarkably stable at ambient conditions. The UV-Vis(-NIR) electronic transitions in parent (**ICz-CN**)$_2$ and **ICz-CN** and their different redox forms have been assigned convincingly with the aid of TD-DFT calculations. The σ-bond cleavage in neutral (**ICz-CN**)$_2$ is achieved in solution and in the solid-state upon soft external stimuli (temperature, pressure), showing a strong chromism from light yellow to blue−green. Notably, in the solid state, the predominant formation of the monomeric diradical species is achieved under high hydrostatic pressure (>1 GPa).

---

[1] Work conducted when Miriam Peña-Alvarez was a team member of MALTA-Consolider Team, Department of Physical Chemistry I, Chemistry Faculty, University Complutense of Madrid, 28040 Madrid, Spain

Introduction

Chromo-active materials have attracted much interest of the scientific community in different fields as they are able to reversibly change colour when (i) exposed to certain light energies (photochromic switches)[1,2], (ii) slightly deformed with small compressive strain[3,4] or (iii) lightly heated/cooled.[5-7] The reversible homolytic covalent bond cleavage/formation involving radical species has been recently demonstrated to be an efficient strategy to obtain multi-responsive chromic soft materials.[5-15] Owing to this property, organic mono- and diradicals have emerged as essential building blocks in Dynamic Covalent Chemistry (DCC).[16-18] The unique feature of the open-shell systems to form weak self-assembled molecular complexes has earmarked organic radicals as prospective for a great number of applications such as stimuli-responsive soft materials,[5-7] spintronics[19] , spin cross-over materials[20,21] or molecular self-assembly.[22]

Currently, several dicyanomethylene-substituted compounds have been identified to undergo reversible σ-oligomerization through the formation of long $(CN)_2C–C(CN)_2$ σ-bonds, giving rise to cyclophanes and other macrocyclic compounds.[3,5-7,11,15,23-28] For instance, our teams have found that carbazole-based diradicals are able to form stable cyclophane macrocycles upon soft external stimuli, showing a strong chromic effect from violet to white.[6] In another recent study, we have explained how the different substitution positions of the dicyanomethylene groups affect the self-assembly of carbazole-based diradicals.[7] Meta-substituted cyclophanes were found to dissociate harder both in solution and in the solid state when compared to para-substituted carbazole homologues, as a result of the formation of more stable macrocycles with shorter C−C bonds in the bridge. However, a fundamental understanding of how an enlargement of the conjugated core affects the intermolecular σ-bonding reactivity of carbazole-based diradicals is still missing.

It is worth noticing that particularly indolocarbazole-based systems have been studied in depth because of their promising properties, viz.: (i) good planarity and rigid conjugated core, which can increase the charge transport properties by improving intermolecular interactions reflected in better molecular packing arrangements; (ii) high thermal stability; (iii) prominent photophysical and electrochemical properties, such as wide band gap and low-lying HOMOs, which outlines them as promising materials for organic electronics.[29-35]

Hitherto, five different indolocarbazole isomers have been distinguished by the position and orientation of the nitrogen atom corresponding to the indole moiety change (see Figure S1). Although other possible configurations also exist, these are rather rare and usually not incorporated in the "classical" indolocarbazole concept.[36] In particular, the chemistry of indolo[3,2-b]carbazole has frequently been reported in the literature,[37-41] evidencing a quinoidal character for its ground state[42,43] and an easy modulation of their properties by the insertion of functional groups.[44-48] However, the introduction of dicyanomethylene terminal groups, a well-known strategy to stabilize diradical species, has not been explored so far in these materials. All these properties make indolocarbazole-based systems ideal test-bed molecules for the design of new diradical compounds.

In the present work, we have synthesized and characterized an indolo[3,2-b]carbazole compound containing terminal dicyanomethylene groups in the 3,9-positions, abbreviated as **ICz-CN**, which is capable of forming a σ-dimer structure with two co-facial

2

indolocarbazole units featuring attractive π-π interactions (Figure 1). Our study will focus on the relation between the diradical character of the open-shell monomer and its σ-oligomerization, also referred to as the cyclophane formation (**ICz-CN** to **(ICz-CN)₂**). In addition, the reversibility of the monomer/cyclophane transformation will also be explored both in: (i) solid state by varying the external stimuli (temperature and pressure), and (ii) in solution where solvents of different polarity and cyclic voltammetry will be employed to infer the molecular connectivity. A combined experimental and theoretical approach to reach the goals will couple a range of spectroscopic and electrochemical techniques with density functional theory (DFT) calculations.
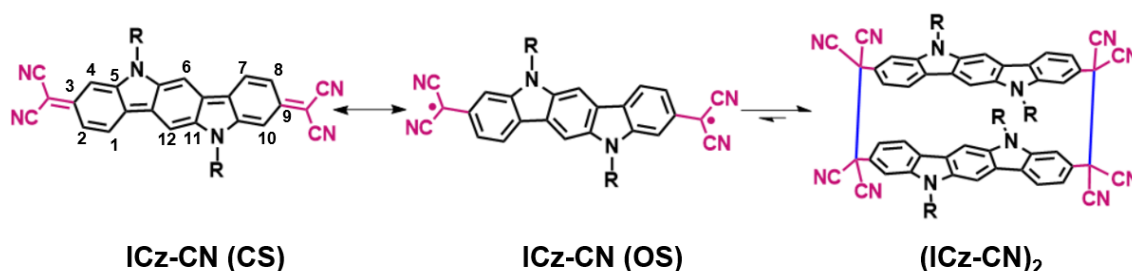
*Figure 1. Equilibrium between the isolated monomer **ICz-CN** and its corresponding σ-dimer (**ICz-CN**)₂. The singlet ground state of **ICz-CN** is presented as a resonance between the closed-shell (CS) state (left) and the open-shell (OS) diradical state (middle).*

Results and Discussion

1. Syntheses

The synthetic route to **ICz-CN** and the σ-stacked dimer **(ICz-CN)₂** is shown in Scheme 1 (see Supporting Information for the complete experimental details). In the initial step, 3,9-dibromo-indolo[3,2-b]carbazole (**ICz-Br**) reacted with malononitrile through a typical Pd-catalysed Takahashi coupling reaction to afford precursor **1**. After oxidation of **1** with 2,3-dichloro-5,6-dicyanobenzoquinone (DDQ), **ICz-CN** was obtained and concomitantly dimerized in part to **(ICz-CN)₂** in solution due to its active diradical character. Similar to our previously reported[6] 2,7-dicyanomethylene-9-(2-ethylhexyl)carbazole diradical, **Cz-CN** (see Figure S2), an equilibrium exists between **ICz-CN** and **(ICz-CN)₂** in solution, with the dominant the dimer contribution evidenced by electronic absorption spectroscopy at variable temperature, UV-Vis-NIR spectroelectrochemistry and HPLC results (see Figure S4) in connection with DFT and TD DFT calculations (see the discussion in the relevant sections below).

3

Scheme 1. *The synthetic route to diradical **ICz-CN** in equilibrium with the corresponding cyclophane **(ICz-CN)₂**.*

2. Cyclophane Structural Features

The reactive diradicals can form linear polymer or cyclophane structures. The long retention time of GPC (see Figure S4) excludes linear polymerization of **ICz-CN** diradical. **ICz-CN** compounds and its precursor **ICz-Br** were examined by diffusion NMR techniques. Diffusion-ordered spectroscopy (DOSY) experiments were carried out at **ICz** compound concentrations below 2 mM, which corresponds to a dilute regime where the intermolecular separation avoids aggregate formation. Diffusion coefficients (D) were determined and used to estimate the size of the molecules in solution, by calculating the hydrodynamic radius (R_h) using the Stokes-Einstein equation: $R_\mathrm{h} = k_B T/6\pi\eta D$, where k_B is the Boltzmann constant, T is the temperature and η is the kinematic viscosity of the solution.[49,50]

Larger structures diffuse more slowly in solution, showing smaller diffusion coefficients. As can be observed in Table 1, (**ICz-CN**)$_2$ presents a smaller diffusion coefficient than **ICz-Br** and, for instance, a higher R_h value. This indicates that the estimated size of the CN derivative is roughly more than twice larger than that of the Br derivative, in line with the formation of a dominant dimeric structure in the case of **ICz-CN**. This is in good analogy with the well-known trend in diradical systems to form weak and long C−C single bonds in the process of co-facial coupling between the radical centres, giving rise to the formation of σ-aggregates.[7,23,51]

Table 1. *Diffusion coefficients (D) and hydrodynamic radii (R_h) determined by diffuse NMR experiments.*

Compound	D (m²s⁻¹)	R_h (Å)
ICz-Br	$4.05 \cdot 10^{-10}$	10
(**ICz-CN**)$_2$	$1.76 \cdot 10^{-10}$	23

With the aim of predicting the most favourable intermolecular arrangement of the σ-dimer aggregate, we performed DFT calculations for different dimer conformations[52] (Figure 2a): (i) an antiparallel arrangement of the two **ICz-CN** chains; and (ii) a parallel orientation with co-facially superimposed units, thereby maximizing the orbital overlap between the

π-conjugated cores.[53] The calculated free energies revealed that **ICz-CN** is able to form a pancake dimer structure resulting from attractive π-π interactions between two indolocarbazole backbones (see Figure 2a and Figure S5). When comparing the two dimer models, the formation of the antiparallel configuration (Figure 2a, top) is found to be 17 kcal mol^{-1} more favourable than the parallel one. In addition, the formation of the long-strained σ-CC bonds between two radical centres has been monitored by calculating the potential energy curve of the dimerization (Figure 2b), which shows a well-defined minimum at 1.65 Å and changes the curvature around 2.0-2.1 Å. This calculated C–C bond is significantly elongated as compared to canonical $C(sp^3)$–$C(sp^3)$ bonds (1.54 Å). The σ-bonding between the chains causes the hybridization of the dicyano groups to change from the planar sp^2 π-character to sp^3.[54] The negative estimated energy for the formation of this long C–C single bonds (*i.e.*, -67.8 kcal mol^{-1}) is in agreement with the spontaneous dimerization observed experimentally.
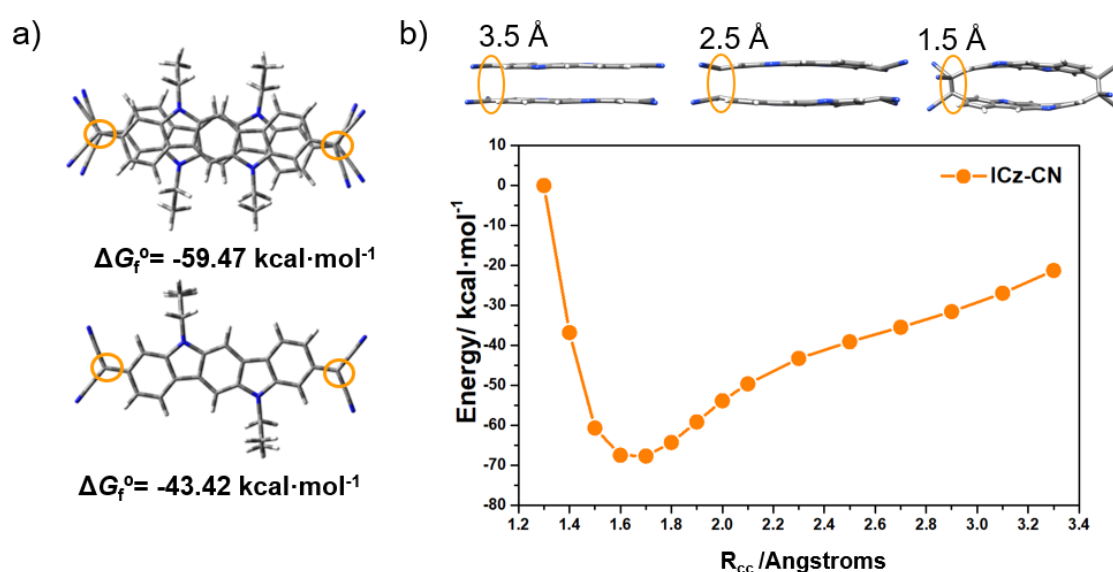

Figure 2. *(a) DFT-calculated global-minimum structure for (**ICz-CN**)$_2$ in two different configurations: antiparallel (up) and parallel (down) for the spatial arrangement of the two isolated monomers. Free energy-of-formation values (at 298 K), calculated at the UM06-2X-D3/6-31G** level, are also shown. (b) Potential energy curve, computed at the UM06-2X/6-31G** level, for (**ICz-CN**)$_2$. Here R$_{CC}$ is the length of the C–C σ-bonds formed between two **ICz-CN** monomers.*

3. Diradical Character Investigation

To gain a deeper insight into the electronic structure and the diradical character of the **ICz-CN**, geometry optimizations at the density functional theory (DFT) level were carried out. Herein, the HOMO and LUMO distributions from the closed-shell state exhibit a delocalization over the whole π-conjugated backbone. Comparing the **ICz-CN** compound with its short-chain analogue **Cz-CN**,[6] the elongation of the conjugated core causes the destabilization of the HOMO while the LUMO is slightly affected (as shown in Figure 3a). Consequently, the energy gap decreases[55] which, nevertheless, may head to relatively smaller ΔE_{ST} values (5.21 eV in **Cz-CN** *vs* 1.66 eV in **ICz-CN**, see Table S1); note that **ICz-CN** is an open-shell diradical in the ground electronic state as in the case of **Cz-CN**. The singly occupied molecular orbital (SOMO) profiles of the α and β spatial distribution

present a typical disjointed feature and the resulting spin density distribution, which has a central symmetry, is highly distributed through the whole **ICz** core with a strong contribution from the dicyanomethylene groups (see Figure 3b and 3c). The high spin density over the bridgehead carbon atoms suggests that the connection between the unpaired electrons of the dicyanomethylene groups at the different **ICz-CN** halves should be favoured as a consequence of the increased diradical character.[7] The optimized structure of **ICz-CN** reveals that the closed-shell form presents a quinoidal character whereas the open-shell singlet state displays a certain degree of aromatization, mainly localized on the central phenylene ring and the adjacent pyrrole groups (see the calculated bond lengths shown in Figure 4a) which might act as the driving force for the stabilization of the diradical species.
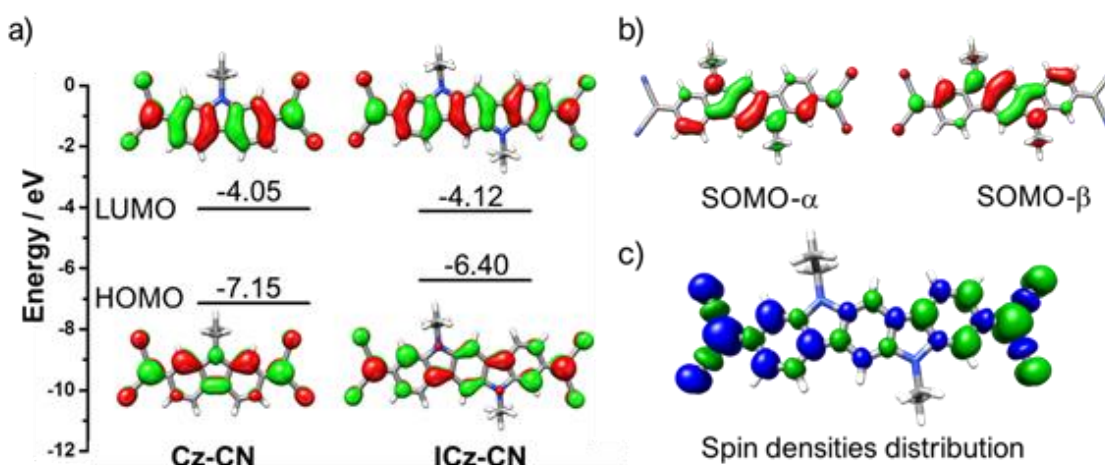
*Figure 3. (a) DFT-calculated molecular orbital diagram for **ICz-CN** and **Cz-CN**, the short-chain analogue at the M06-2X/6-31G** level of theory. (b) Calculated SOMO of α and β electrons and (c) spin density distribution in the diradical singlet ground state of **ICz-CN** at the UM06-2X/6-31G** level of theory with an iso-surface value of 0.03 a.u.. The blue and green surfaces represent α and β spin densities, respectively.*

We now shall address the diradical character of the **ICz-CN** compound which gives a quantitative evaluation of its open-shell singlet nature. This parameter was obtained by using the following methods: (i) through the occupation number of the lowest unoccupied natural orbital (LUNO) ($0 < y_0 < 1$, where $y_0 = 0$ represents a closed-shell state and $y_0 = 1$ represents a pure diradical state), (ii) from the spin-projected formalism, and (iii) using the fractional orbital density (FOD) analysis where the number of strongly correlated electrons in the system is measured. For **ICz-CN,** we obtained values of $N^{FOD} = 1.95$ together with $y_0 = 0.79$ and $y_0 = 0.61$, without and with spin-projected correction, respectively. However, note that smaller N^{FOD} and y_0 values (*i.e.*, 1.31 and 0.49, respectively) are predicted for the related carbazole, **Cz-CN**, system.[6] A linear relationship between the experimental diradical character and the N^{FOD} values was described by Bauer and co-workers for some polyaromatic hydrocarbons (PAHs),[56] as shown in Figure S6. These data reveal that N^{FOD} values larger than 1.5 confirm a greatly pronounced diradical character. In addition, the FOD-density plot, shown in Figure 4b, displays a strong contribution from the carbon atoms of the dicyanomethylene groups which support the radicals in the open-shell resonance structure. In summary, this strong diradical character together with the small above-mentioned OS singlet–triplet gap indicates a very weak coupling between the two radical sites in **ICz-CN**.

6
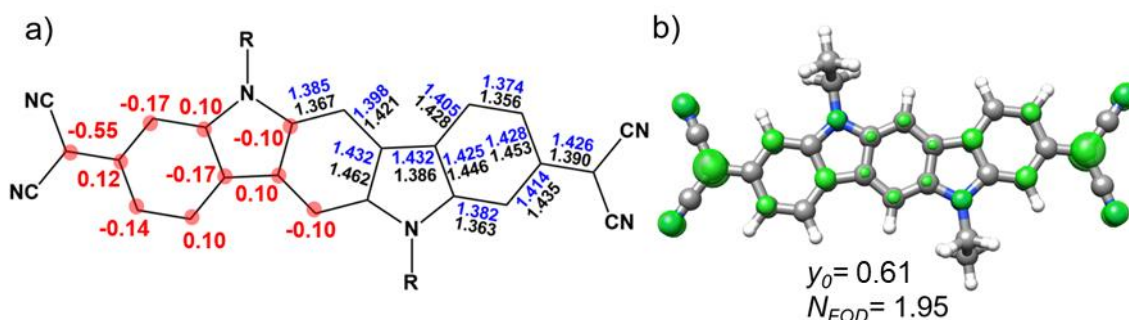
*Figure 4. (a) Calculated bond lengths (Å) for the closed-shell (black data) and open-shell singlet (blue data) diradical forms of the ground electronic state of **ICz-CN**. The numbers given in red denote the spin densities at the specific carbon atoms. (b) Isocontour plot of the FOD density ($\sigma = 0.005$ e·bohr^{-3}) and predicted NFOD values for **ICz-CN**. The diradical character y_0 values calculated at the (U)M06-2X-631G** level is also shown.*

When comparing ^{1}H NMR spectra **ICz-Br** with that of (**ICz-CN**)$_2$ (Figure S3) the proton signals of the σ-aggregate are slightly broader, which is ascribed to the presence of a small amount of the open-shell diradical form of monomer **ICz-CN**. In line with further dissociation of (**ICz-CN**)$_2$ to monomer **ICz-CN** at high temperature, in tetrachloroethene (as discussed below), the proton signals in at low field broaden gradually and disappear at 130 °C. Notably, the original spectrum is fully recovered after cooling down the solution back to room temperature.

4. Cyclophane/monomer interconversion in solution

A. Optical properties

Aiming to analyze the influence of different solvents to isolate the monomers, the optical properties of the target samples were monitored by UV-Vis absorption spectroscopy. First, we checked the response as a function of time when the dimer is dissolved in chloroform. As seen in Figure 5a, the freshly prepared chloroform solution displays: i) strong bands in the UV region and medium-weak bands below 500 nm which corresponds to the cyclophane aggregates, and ii) a small and broad absorption at around 700 nm which is ascribed to the isolated monomer. The spectral profile is slightly affected as a function of time.

Second, we investigated the cyclophane/monomer interconversion upon heating. To this end, we dissolved the indolocarbazole compound in toluene (Figure 5b) and heated the solution from 300 K to 380 K. This induces an increase in the intensity of the **ICz-CN** monomer structured band at 700 nm. Nevertheless, the strongest intensity gain of the monomer low-energy visible band was achieved in o-dichlorobenzene (o-DCB) and tetrachloroethane upon heating (see Figure 5c and Figure S7b, respectively). In fact, almost complete disappearance of the intense UV absorption corresponding to the cyclophane aggregate (**ICz-CN**)$_2$ is achieved while the **ICz-CN** monomer absorption dominates in the spectrum. Visually, the rupture of the long C–C σ-bonds in the aggregate upon heating is accompanied by a gradual change of the solution colour from light yellow to blue-green, which is fully reversed by cooling down the solution back to 300 K (Figure 5d and Figure S8). A similar behavior was recorded in tetrachloroethane (Figure S7b). On the other hand, the diradical monomer formation was hampered in chlorobenzene and 2-methyltetrahydrofuran (Figure S7). Based in these observations,

7

o-DCB was selected for the temperature-controlled cyclic voltammetric study of (**ICz-CN**)$_2$ and **ICz-CN** presented in the following section.
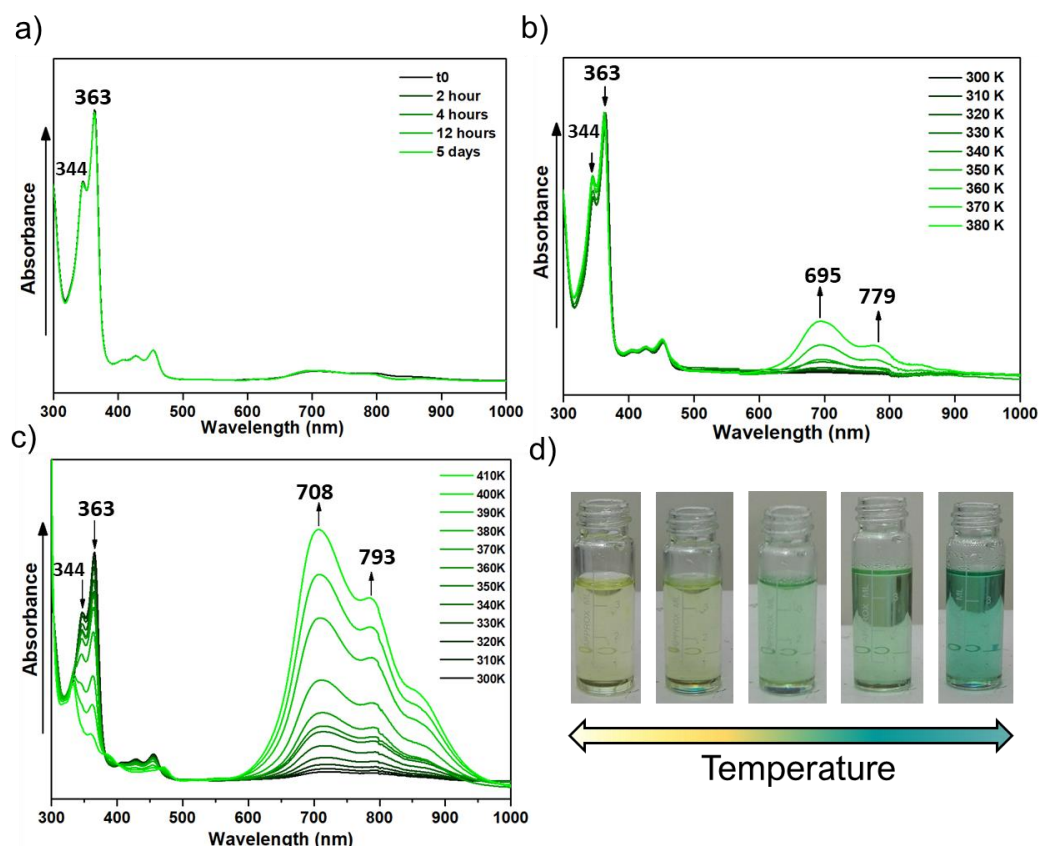
Figure 5. *(a) UV-Vis absorption of the freshly prepared solution of (**ICz-CN**)$_2$ in chloroform at room temperature as a function of time. (b) UV-Vis-NIR spectral changes accompanying the thermal conversion of (**ICz-CN**)$_2$ to monomer **ICz-CN** in toluene upon heating. (c) UV-Vis-NIR spectral changes accompanying the nearly complete transformation of (**ICz-CN**)$_2$ to **ICz-CN** in o-dichlorobenzene (o-DCB) as a function of temperature. (d) Gradual and reversible colour change from light yellow to blue-green upon heating, which reflects the spectral changes in (c).*

TD-DFT calculations eminently support the experimental UV-vis spectral evolution when going from the co-facial σ-dimer (**ICz-CN**)$_2$ to the isolated monomer **ICz-CN** (Figures S9 and S10). While a moderate electronic transition at 302 nm together with two less intense transitions at 352 and 371 nm are predicted for (**ICz-CN**)$_2$ corresponding to S$_0$ → S$_5$, S$_0$ → S$_2$ and S$_0$ → S$_1$ transitions, respectively, that involves orbitals with π-character delocalized through the two indolocarbazole moieties, an intense electronic transition at 703 nm is predicted for the isolated monomer **ICz-CN**, which is ascribed to the S$_0$ → S$_2$ transition with a strong π−π* character (HOMO→LUMO). These results are in good agreement with the HOMO-LUMO gap strongly decreasing when going from (**ICz-CN**)$_2$ to **ICz-CN** (Figure S11). Interestingly, the UV-Vis spectrum predicted for the precursor **ICz-Br** resembles that of the aggregate (**ICz-CN**)$_2$. This is in consonance with the similar energy levels and topologies of the frontier molecular orbitals of **ICz-Br** and (**ICz-CN**)$_2$ (Figures S10 and S11), which suggest an aromatic-to-quinoidal transformation of the π-conjugated indolocarbazole unit upon the HOMO–LUMO optical excitation, whereas an opposite quinoidal-to-aromatic transformation takes place in **ICz-CN** (Figure 3).

8

B. *Redox properties*

Redox properties of the **ICz-CN** species, existing at ambient conditions in the dominant cyclophane-type dimeric form, (**ICz-CN**)$_2$, were investigated with cyclic voltammetry in dichloromethane (DCM) at 298 K (Figure 7), and in 1,2-dichlorobenzene (o-DCB) at 298 and 393 K (Figure S12b). Precursor **ICz-Br** was also measured as the reference system (Figure 6 and Figure S12a, respectively). The redox potentials are summarised in Table 2.

For reference **ICz-Br** in DCM, two reversible one-electron oxidations, O1 and O2, are observed at $E_{1/2}$ = +0.45 and +1.09 V against Fc/Fc$^+$ (Figure 6). Figure S10 reveals that the π HOMO of **ICz-Br** is fully delocalized over the ICz backbone. The inherent stability of [**ICz-Br**]$^+$ and the corresponding dication has been confirmed by spectroelectrochemical experiments described in the following section. The reversible oxidation of (**ICz-CN**)$_2$ is shifted positively by 180 mV (Figure 7), which can be attributed to the electron-withdrawing effect of the terminal dicyanomethylene groups, despite their negligible contribution to the HOMO character (Figure S10). This shift is in a good agreement with the slight stabilization of the HOMO when going from **ICz-Br** to (**ICz-CN**)$_2$ (Figure S11). The second oxidation of (**ICz-CN**)$_2$ was not observed within the anodic potential window of the DCM electrolyte. The HOMO of the dimer is delocalized over both σ-bound and π-interacting ICz backbones, which debars the assignment of [(**ICz-CN**)$_2$]$^+$ as a redox-asymmetric, mixed-valence species. A strong supportive evidence for this statement has been obtained from the analysis of the UV-Vis-NIR absorption of the cationic product supported by TD-DFT calculations.

The anodic behaviour of (**ICz-CN**)$_2$ and reference **ICz-Br** remain unchanged in o-DCB at 298 K. At 393 K, yellow (**ICz-CN**)$_2$ is fully converted to green diradical **ICz-CN** (Figure S13). The oxidation wave of the monomer becomes irreversible whilst the stability of singly oxidized [**ICz-Br**]$^+$ is preserved at the high temperature. No spectroelectrochemical evidence for the likely decomposition of [**ICz-CN**]$^+$ could be obtained with the experimental setup in use.

Diradical **ICz-CN** formed in o-DCB at 393 K (Figure S12b) undergoes two reversible cathodic steps at $E_{1/2}$ = -0.46 and -0.67 V, while no reduction of reference **ICz-Br** was encountered in this cathodic region (Figure S12, left). This difference correlates with the strong stabilizing effect of the dicyanomethylene terminal groups on the LUMO of **ICz-CN**, as determined by DFT calculations (Figure S11).

The DFT calculations suggest that dimer (**ICz-CN**)$_2$ reduces more negatively compared to **ICz-CN** (Figure S11). However, the cathodic CV response of the dimer is not straightforward (Figure 7). The reduction process is indeed shifted below -1 V but appears as poorly resolved at the initial cathodic scan. This is likely a consequence of a dynamic behaviour of (**ICz-CN**)$_2$ that exists in equilibrium with diradical **ICz-CN** also at ambient temperature (see the preceding NMR and HPLC/GPC results, and the EPR spectrum in Figure S23 and EPR discussion in the Supporting Information). In the neutral parent state, the equilibrium is largely shifted towards the dimer (Figure S4a) but the initial reduction of the minor **ICz-CN** component is still detectable during the initial cathodic scan as a small wave at ca. -0.8 V (see Figure 7, left). When passing the potential interval between -1 V and -2 V, the cyclophane structure dissociates upon the reduction and the radical anionic and dianionic forms of **ICz-CN** are generated. This cathodic process is much better resolved in the corresponding thin-layer cyclic voltammogram of (**ICz-CN**)$_2$ (Figure S15), which testifies to the consumption of two electrons (in comparison with the reversible one-electron anodic wave). On the reverse

9

anodic scan, two close counterwaves are observed between -0.8 V and -0.6 V, which resembles the high-temperature cyclic voltammogram of dissociated **ICz-CN** (Figure S12). The reversibility of the two one-electron cathodic steps was confirmed by UV-Vis-NIR spectroelectrochemistry described in the following section. Importantly, cycling the voltametric scan of (**ICz-CN**)$_2$ between 0 V and -2 V rises the cathodic wave at ca -0.8 V (Figure 7, right) due to the reduction of biradical **ICz-CN** prior to its conversion to neutral cyclophane (**ICz-CN**)$_2$. The dimer reduces under these experimental conditions between -1.2 V and -2 V, as revealed by the gradually decreasing cathodic current in this potential interval. In summary, the cathodic behaviour of (**ICz-CN**)$_2$ in equilibrium with **ICz-CN** is far from trivial but the assignment is consistent with the CV response of **ICz-CN** at high temperature and the thin-layer spectro-electrochemical data complemented with TD-DFT calculations (see the following section).
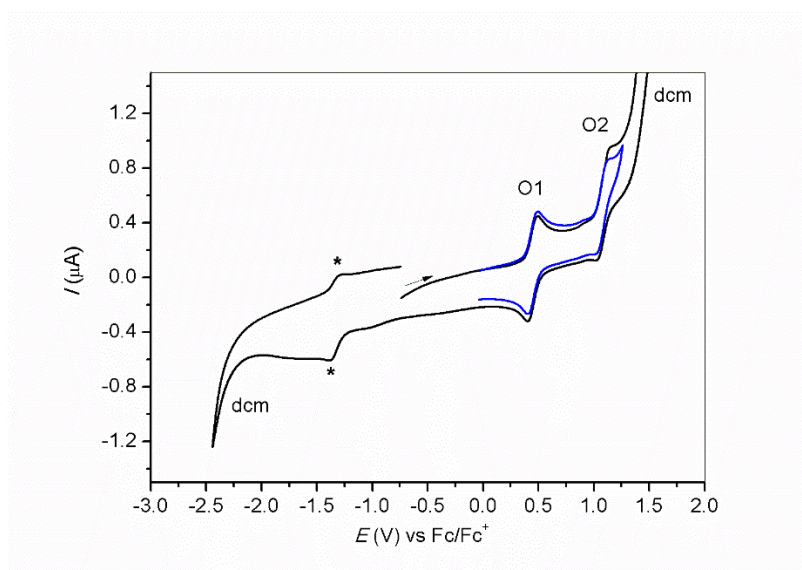
Figure 6*. Cyclic voltammograms of 10^{-3} M **ICz-Br** (blue and black curves) in dichloromethane/Bu$_4$NPF$_6$ at a Pt microdisc electrode and v = 100 mV s^{-1} and T = 298 K. The standard ferrocene/ferrocenium cobaltocene/cobaltocenium redox couple (at -1.33 V, asterisks) was used as the internal reference. The labels 'dcm' denote the anodic and cathodic limits of the electrolyte.*
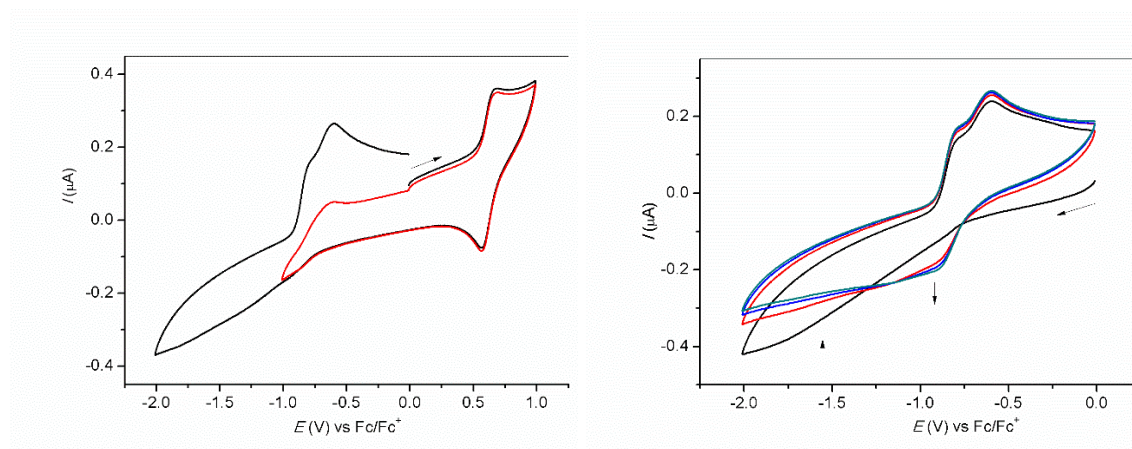
Figure 7*. Cyclic voltammograms of 10^{-3} M (**ICz-CN**)$_2$ in dichloromethane/Bu$_4$NPF$_6$ at a Pt microdisc electrode and v = 100 mV s^{-1} and T = 298 K. Left: anodic and cathodic scans. Right: repeated cathodic scan (4 cycli – black, red, blue, and green).*

10

Table 2. Redox properties of **ICz-Br,** isolated monomer **ICz-CN** and cyclophane-type dimer (**ICz-CN**)$_2$ determined by cyclic voltammetry at a Pt microdisc electrode.

Compound	$E_{1/2}(1)$ / V	$E_{1/2}(2)$ / V	$E_{1/2}(3)$ / V
ICZ-Br	0.45 (O1) [a]	1.09 (O2) [a]	-
	0.44 [b]	1.08	-
	0.45 [c]	[d]	-
(**ICZ-CN**)$_2$	0.63 [a]	[d]	[a,e]
	0.60 [b]	[d]	-
ICZ-CN	0.70 [c,f]	[d]	-0.46, -0.67 (R1, R2) [c]

[a] Dichloromethane/Bu$_4$NPF$_6$ at T = 298 K. [b] o-Dichlorobenzene/Bu$_4$NPF$_6$ at T = 298 K. [c] o-Dichlorobenzene/Bu$_4$NPF$_6$ at T = 393 K. [d] Beyond the anodic potential limit of the electrolyte. [e] Poorly resolved, below -1.2 V vs Fc/Fc$^+$. [f] $E_{p,a}$ value; irreversible oxidation.

C. UV-Vis-NIR Spectro-electrochemistry

To further probe the nature of the redox steps at ambient temperature pertaining to the indolocarbazole species, cyclophane (**ICz-CN**)$_2$ and reference **ICz-Br**, UV-Vis-NIR spectroelectrochemistry in DCM was implemented.[57] Table 3 summarises the positions of electronic absorption maxima for both species in the varying oxidation states.

Table 3. Electronic absorption of **ICz-Br** and (**ICz-CN**)$_2$, and their stable redox forms in DCM at 298 K.

Compound	ICz-Br	(ICz-CN)$_2$
Neutral Parent	290, 333, 350, 402, 422	296, 346, 364, 427, 456
Radical Cation	324, 342, 404, 871	328, 348, 411, 852
Dication	314, 609	-
Radical Anion [a]	-	292, 451, 570
Dianion [a]	-	290, 442, 568

[a] Corresponds to stable reduced monomer **ICz-CN**.

11

The reversible UV-Vis spectral changes accompanying the smooth two-step oxidation of reference **ICz-Br** to the corresponding monocationic and dicationic states (Table 3) are shown in Figures S16 and S17, respectively. The same isosbestic points are maintained during the corresponding reverse cathodic steps and the intermediate cationic and parent absorptions are fully recovered. The experimental electronic absorption of [**ICz-Br**]+ in the UV-Vis-NIR is plausibly reproduced by TD-DFT calculations (Figure S18, Table S3).

Exploring the reversible one-electron oxidation of the cyclophane dimer (**ICz-CN**)$_2$, a very similar spectroscopic response is seen in Figure 8. This observation specifically regards the appearance of the new structured absorption band at 328/348/411 nm and the NIR absorption maximum at *ca.* 852 nm. These absorption features are fairly well reproduced by TD-DFT calculations on [(**ICz-CN**)$_2$]+ (Figure S18). The dimer cation does not absorb between 500-600 nm, differently from [**ICz-Br**]+ that shows a weak absorption in that region (Figure S16). In contrast, strong absorption around 500 nm has been predicted for singly oxidized monomer [**ICz-CN**]+ (Table S3). Thus, the recorded experimental electronic absorption spectra (Figure 8) comply with the dimeric cyclophane structure preserved at ambient temperature also in the oxidized product, in line with the reversible nature of the anodic process (see Figure S15). Both [**ICz-Br**]+ and spin-delocalized [(**ICz-CN**)$_2$]+ (cf. the HOMO of the parent compound in Figure S10) apparently feature similar chromophores largely independent of the terminal substituents. This coincidence has a likely origin in the similar aromatic nature of the ICz backbone in both compounds, as the CN groups are no longer π-conjugated with the ICz core upon the formation of the long C–C σ-bonds.
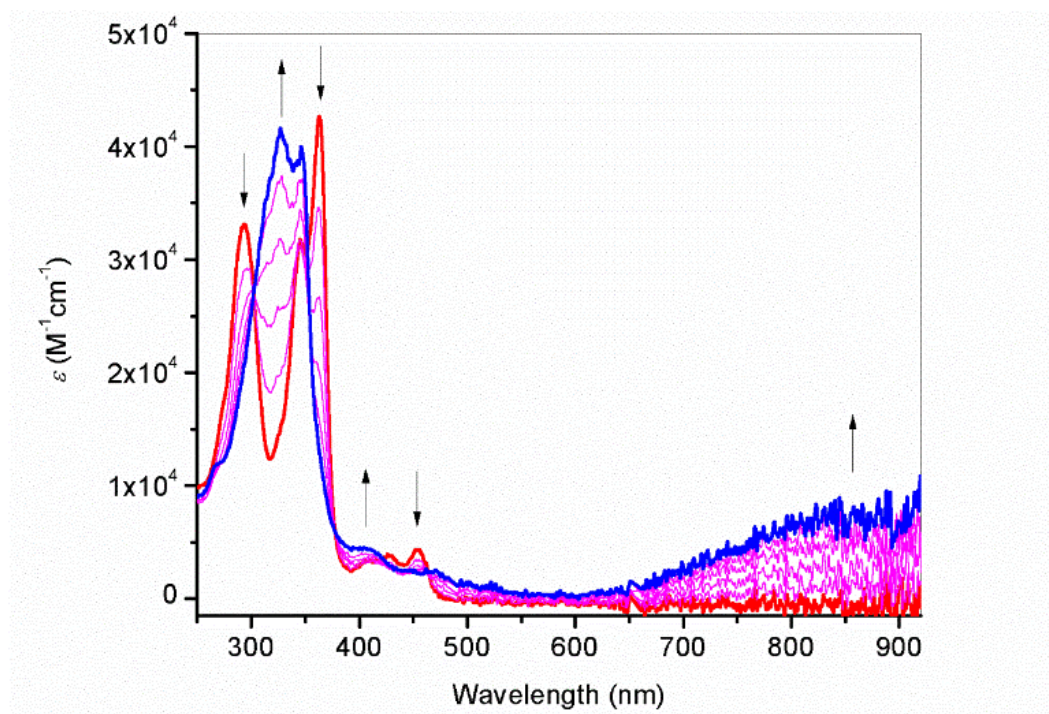
Figure 8. UV-Vis spectral changes recorded during the reversible oxidation (**ICz-CN**)$_2$ - e⁻ → [(**ICz-CN**)$_2$]+ in CH$_2$Cl$_2$/10⁻¹ M Bu$_4$NPF$_6$ at 298 K within an OTTLE cell.

12

In contrast to **ICz-Br**, diradical **ICz-CN** is reducible in two fully reversible one-electron steps at low overpotentials (Table 2). At ambient temperature, **ICz-CN** presents only a minor component in the equilibrium with the cyclophane dimer (Figure S4a) and its conventional CV could only be recorded at sufficiently high temperatures where the cyclophane dimer fully dissociates (Figure S12). The thin-layer CV of (**ICz-CN**)$_2$ recorded in dichloromethane at ambient temperature (Figure S15) showed two close-lying cathodic waves at lower electrode potentials, between -1V and -2V, resembling the cathodic response of (**ICz-CN**)$_2$ whose LUMO is lying higher compared to **ICz-CN** (Figure S11). As argued in the preceding CV section, the cathodic spectroelectrochemistry of (**ICz-CN**)$_2$ in fact starts with the reduction of the minor diradical component at ca -0.8 V (Figure 7), breaking the equilibrium and converting the dimer completely to the singly reduced monomer, [**ICz-CN**]$^-$. The resolved second cathodic step then produces stable [**ICz-CN**]$^{2-}$. The corresponding UV-Vis spectral changes accompanying both reduction steps are depicted in Figure 9. The presence of isosbestic points excludes any side reaction. A full recovery of the parent dimer absorption was observed after the stepwise reoxidation of [**ICz-CN**]$^{2-}$ (Figure S15). The anion [**ICz-CN**]$^-$ features a new strong and broad absorption band with a maximum at 451 nm, and a weaker absorption at 570 nm. This visible absorption persists also in the dianion [**ICz-CN**]$^{2-}$ but both the intensity and bandwidth are affected. Electronic transitions of [**ICz-CN**]$^-$ and [**ICz-CN**]$^{2-}$ in the near UV-visible region calculated with TD-DFT (Figure S18) are consistent with the experimental spectra, reproducing the intense electronic absorption around 450 nm measured for [**ICz-CN**]$^-$ and its increased intensity when generating [**ICz-CN**]$^{2-}$. The weak absorption features of both reduced forms of **ICz-CN** between 500-650 nm were, however, not reproduced. On the other hand, the modelled reduced dimers, [(**ICz-CN**)$_2$]$^{n-}$ (n = 1, 2), differ considerably in the calculated electronic absorption, showing strong low-energy absorptions at 864 nm (anion) and 708 nm (dianion) not encountered in the experimental spectra. The combined voltammetric and spectral evidence leads to the conclusion that the cyclophane structure dominates in the solution and ambient conditions only in the neutral state. The cathodic spectroelectrochemistry confirms the existence of the equilibrium between **ICz-CN** and (**ICz-CN**)$_2$ revealed by other methods (Figures S3 and S4), starting with the reduction of the minor monomer component at the characteristic low cathodic overpotential. The broken equilibrium caused by the electron transfer converts the cyclophane dimer readily to the monomer anion that undergoes the second reversible reduction. Reversely, the reoxidation of [**ICz-CN**]$^-$ to the neutral diradical restores the equilibrium with the dominant cyclophane dimer. It would have been even more conclusive to conduct the reversible reduction of isolated diradical **ICz-CN** in *o*-dichlorobenzene at 393 K (Figures S12 and S13) but the experimental setup for this experiment was not at disposal.

13
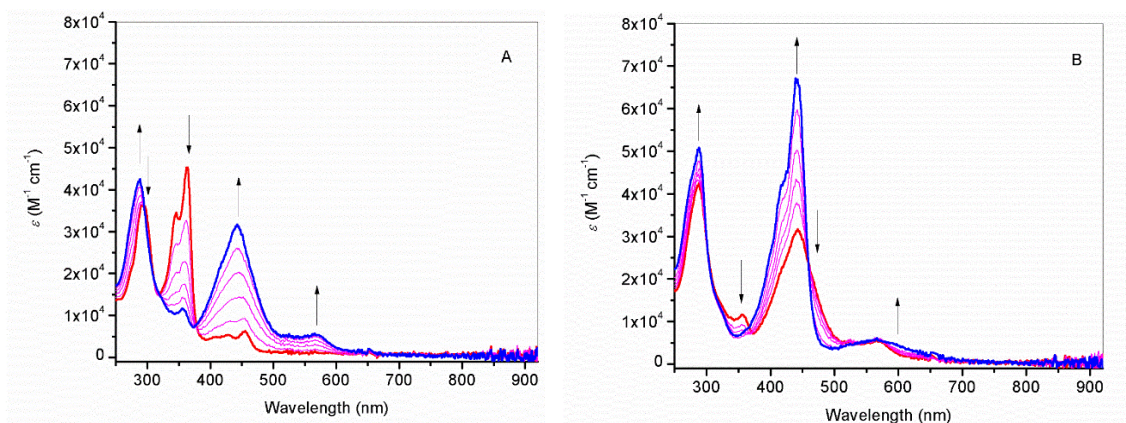
Figure 9. UV-Vis spectral changes recorded during the cathodic steps 1/2 (**ICz-CN**)$_2$ + e$^-$ → [**ICz-CN**]$^-$ (A) and [**ICz-CN**]$^-$ + e$^-$ → [**ICz-CN**]$^{2-}$ (B) in CH$_2$Cl$_2$/10^{-1} M Bu$_4$NPF$_6$ at 298 K within an OTTLE cell.

5. Cyclophane/monomer interconversion in the solid state: temperature and pressure dependence

The C–C σ-bond dissociation in the solid state of the cyclophane dimer was attempted by application of external stimuli such as elevated temperature or pressure. To this end, we have used IR and Raman spectroscopies to probe structural effects causing any mechanochromic changes[6,7,54,58] and for the investigation of the diradical character of quinoidal molecules.[59,60]

Upon application of mechanical stimuli, *i.e.*, grinding of (**ICz-CN**)$_2$ powder with a mortar to prepare a KBr pellet for IR spectroscopy (estimated maximum pressure/stress *ca.* 0.1 GPa), a slight darkening is observed (Figure 10a). This observation suggests that mild pressures have modest impact on the cyclophane dimer/monomer transformation, as further corroborated by IR spectroscopy. The most intense ν(CN) band, attributed to the cyclophane light-yellow powder at ambient conditions, appears centred at 2255 cm^{-1} (similar to non-conjugated nitriles). This band remains prominent in the IR spectrum of the corresponding KBr pellet recorded at both room temperature and 523 K and then cooled down back to room temperature, thus suggesting that the dimer cyclophane structure is always prevalent. However, an additional, weak v(CN) feature appears after grinding at ca. 2224 cm^{-1} which is attributed to the formation of **ICz-CN**, as supported by DFT calculations (Figure 10b), indicating the presence of isolated monomers. In contrast, the σ-aggregates formed by the analogous carbazole-based **Cz-CN** systems dissociate much easier in the solid state[6,7]; this difference is ascribed to the longer conjugated ICz backbones enabling stronger π–π interactions between the co-facially overlapped cores in the pancake (**ICz-CN**)$_2$ aggregates. Also, note that an additional, very weak v(CN) band appears at ca. 2189 cm^{-1} that might be related to the presence of open linear staircase dimers, (**ICz-CN**)$_2$-**op**, as revealed by DFT-calculations (see Figure S19). The formation of staircase oligomers was also found[6,7] in the carbazole-based **Cz-CN** systems, albeit at high pressures. A more detailed investigation is necessary to analyse the oligomerization behaviour of this solid-state system.

14
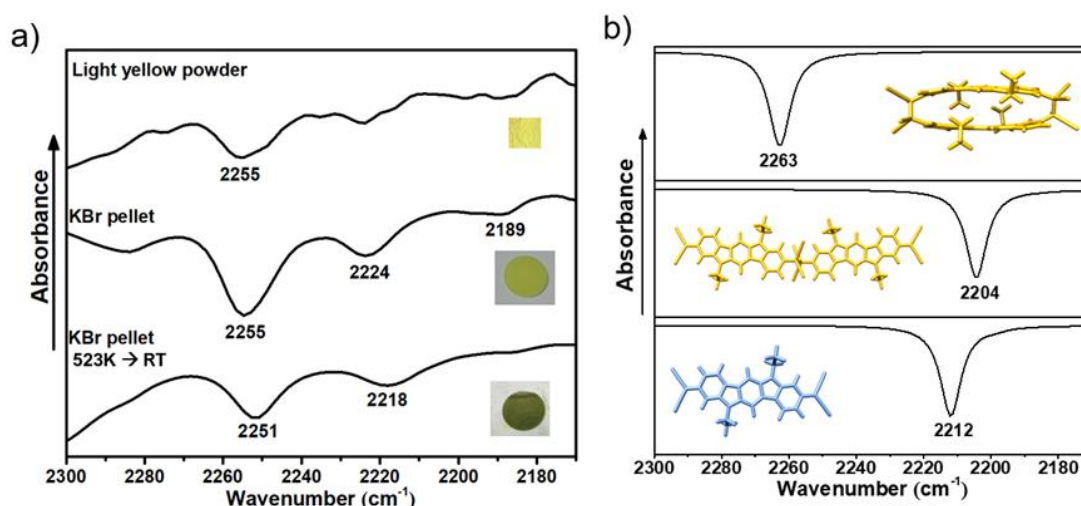
Figure 10. *(a) IR spectrum of (**ICz-CN**)₂ as a light-yellow powder at room temperature (top), a yellow KBr pellet containing a mixture of dimer, open linear oligomer and isolated diradical **ICz-CN** (middle), and the KBr pellet after heating at 523 K (bottom). (b) Theoretical IR spectra of (**ICz-CN**)₂ (top), open linear (**ICz-CN**)₂-**op** (middle) and **ICz-CN** monomer (bottom).*

Figure 11a displays the FT-Raman spectrum of the light-yellow powder corresponding to the (**ICz-CN**)₂ dimer aggregate, and the resonance Raman spectrum of isolated diradical **ICz-CN** in o-DCB at 363 K. When comparing the two spectra, the most pronounced changes are found in the fingerprint region between 1700 and 1100 cm⁻¹. (i) The most intense band of the dimeric structure appears at 1640 cm⁻¹, assigned to a ν(CC) mode of the ICz rings (note that it bears resemblance to that assigned to the aromatic precursor **ICZ-Br** at 1634 cm⁻¹) (ii) Notably, this ν(CC) mode appears at 1580 cm⁻¹ in the isolated monomer, thus suggesting a change in the molecular structure from an aromatic to a more quinoidal character. (iii) The appearance of the band at 1191 cm⁻¹ in the resonance Raman spectrum of hot solution corroborates the presence of the isolated **ICz-CN** monomer structure, as this mode is ascribed to the CH bending of the central phenylene ring being hindered in the dimeric unit. This experimental spectral evolution is in a very good agreement with the theoretical Raman spectra (Figure 11b); for instance, in the calculated spectra of **ICz-CN** the two key bands indicating the diradical monomer formation are predicted at 1574 and 1195 cm⁻¹.

15
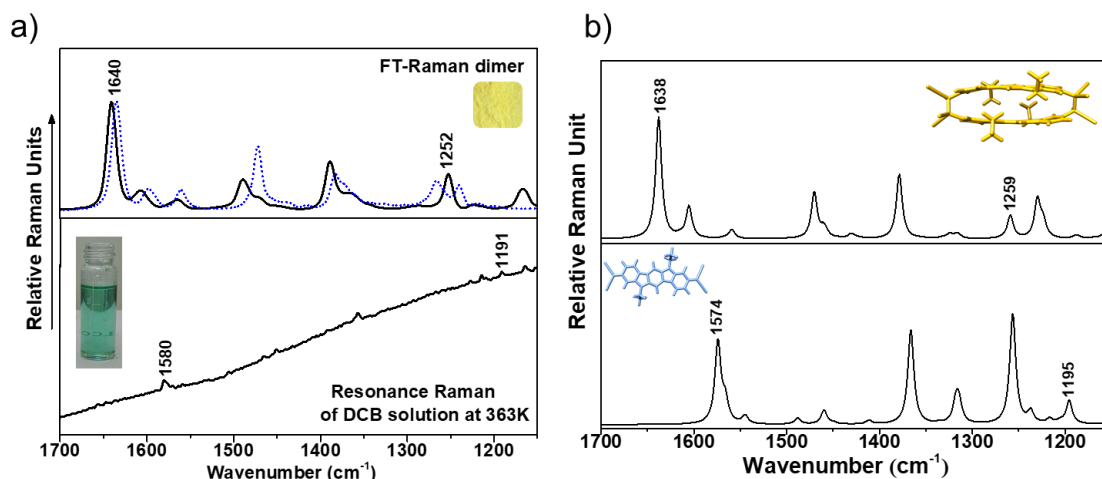
Figure 11. (a) FT-Raman spectra of the solid yellow powder of (**ICz-CN**)$_2$ (black line) an brominated precursor **ICz-Br** plotted as blue dots (top) and the resonance Raman spectrum (λ_{exc} = 785 nm) of isolated diradical **ICz-CN** in o-DCB at 363 K (bottom). (b) Theoretical Raman spectra calculated (M06-2X/6-31G**) for (**ICz-CN**)$_2$ and **ICz-CN.**

The transformation of the dimeric cyclophane structure into the isolated monomers in the solid state could also be monitored when applying pressures raising well above 0.1 GPa in a more controlled way.[61] To this end, (**ICz-CN**)$_2$ was compressed by means of a sapphire anvil cell. As seen in Figure 12, colour changes from light yellow to deep green are observed under the application of pressures in the few GPa range. Raman spectroscopy is an excellent diagnostic tool to evaluate electronic and structural changes in π-conjugated systems, as π-electron density is highly polarizable and consequently, changes in the Raman shift, width and cross section will be highly sensitive to changes in the π–electron density.[62,63] Thus, we now make use of Raman spectroscopy to evaluate the structural changes occurring upon pressure application. As depicted in Figure 12, at compressions reaching *ca.* 2.2 GPa, the Raman spectrum reveals several differences from that at the ambient pressure, suggesting that the dimer C–C bonds are broken, and a monomer configuration is favoured. This assignment is supported by the appearance of new Raman bands at 1585 cm^{-1} and 1140 cm^{-1}. As previously mentioned, the band at *ca.* 1580 cm^{-1} is linked to the ν(CC) stretching mode of the conjugated core in the monomer, while the band at 1140 cm^{-1} corresponds to the *w*(CC) (wagging) mode of the central phenylene unit. The latter mode becomes intense in the monomer because it is not hindered by the neighbouring connecting unit, as observed in the dimer. The formation of monomeric units upon high pressure has been previously reported[6] for the carbazole-based analogue, **Cz-CN**, and its cyclophane tetramer. This effect can be ascribed to the fact that the compression hinders the π-electron delocalization within complex and large molecular skeletons and the radical forms become more dominant.[64,65] For a more detail analysis of the pressure-dependent Raman and emission spectral changes, reflecting the transformation of dimer (**ICz-CN**)$_2$ to isolated monomer **ICz-CN**, see Figures S20-S22.

16
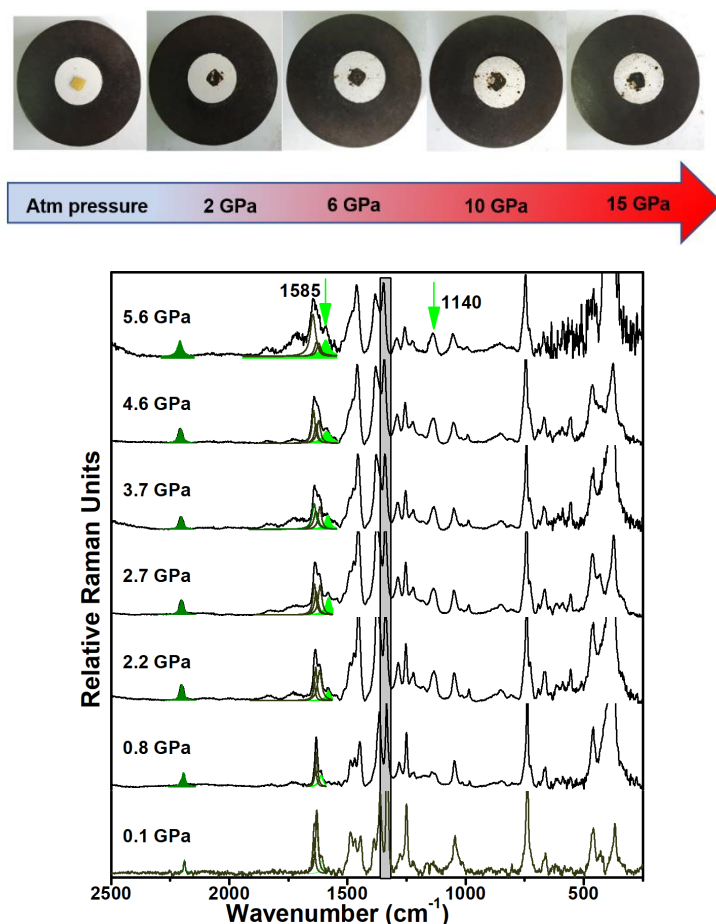
Figure 12. *Colour changes of solid (**ICz-CN**)$_2$ converting to monomer diradical ICz-CN at high pressures (top). Raman spectra of the solid yellow powder of (**ICz-CN**)$_2$ at selected pressures measured using the 785 nm as excitation line (bottom). Marked peaks correspond to: v(CC) stretching mode of the conjugated bonds.*

Conclusions

This work demonstrates for the first time the dynamic covalent properties of indolocarbazole-based diradicals. To this end, we have synthesized a novel indolo[3,2-b]carbazole substituted with dicyanomethyl groups, **ICz-CN**, which is isolated as a stable σ-dimer (**ICz-CN**)$_2$. A dynamic equilibrium between the monomer diradical **ICz-CN** and the dimeric cyclophane, (**ICz-CN**)$_2$, is observed in solution under ambient conditions (with a minor diradical component), as proven by HPLC, NMR and cathodic spectroelectrochemistry. A similar situation exists in the solid state, where **ICz-CN** shows a weak EPR signal. Comparing the **ICz-CN** compound with its short-chain carbazole-based analogue, **Cz-CN**, the elongation of the conjugated core results in an increase of the diradical character together with the small open-shell singlet-triplet gap. The weak cyclophane C–C bonds are susceptible to thermal and mechanochemical cleavage both in the solid state and solution, as demonstrated by combining an exhaustive experimental and theoretical approach. Interestingly, the dynamic cyclophane/monomer interconversion is accompanied by a strong colour change from light yellow to blue-green. In summary, this work has shed light on the challenging dynamic covalent chemistry properties of π-conjugated diradicals and helped to identify new potential design strategies for stimuli-responsive materials.

17

Supporting Information

The following file is available free of charge:
Experimental and Theoretical Methodology; Synthetic details; Related chemical structures; ^{1}H NMR spectra of **(ICz-CN)₂**, compound **1** and **ICz-Br;** HPLC and GPC data; DFT-computed global minimum structure for **(ICz-CN)₂**; Comparison of experimental diradical character (y_0) and the N_{FOD} data; DFT-calculated relative energies for **ICz-CN** and **Cz-CN** and free energy of formation values for **(ICz-CN)₂** and **ICz-CN;** UV-Vis-NIR absorption of solution of **ICz-CN** in different solvents; TD-DFT calculated vertical transition energies and diagram of the frontier molecular orbital energy levels for **ICz-CN, (ICz-CN)₂** and **ICz-Br**; cyclic voltammograms of **(ICz-CN)₂** and **ICz-Br** and thin-layer cyclic voltammogram of (**ICz-CN**)₂**;** Spectroelectrochemical data for **ICz-Br**; TD-DFT calculated vertical transition energies and diagram of the frontier molecular orbital energy levels for **ICz-CN, (ICz-CN)₂** and **ICz-Br** in their reduced and oxidized states; DFT-calculated global minimum structure for open linear dimer (**ICz-CN**)₂-op; Colour changes of **(ICz-CN)₂** converting to **ICz-CN** at high pressures; Theoretical Raman spectra for **(ICz-CN)₂** and **ICz-CN**; Pressure-dependent Raman spectra and photoluminescence spectra at selected pressures of **(ICz-CN)₂** in solid state; discussion about the spectral changes observed in the Raman and emission spectra upon pressure application; X-band EPR spectrum of diradical **ICz-CN** in a solid-state mixture with dominant **(ICz-CN)₂**, and the discussion of the EPR signal.

ORCID

Irene Badía Domínguez: 0000-0002-2736-8943
Miriam Peña Álvarez: 0000-0001-7056-7158
Andrés Pérez Guardiola: 0000-0002-8340-1349
Sandra Rodríguez González 0000-0001-6563-7852
Juan Carlos Sancho García: 0000-0003-3867-1697
František Hartl: 0000-0002-7013-5360
M. Carmen Ruiz Delgado: 0000-0001-8180-7153

Notes

The authors declare no competing financial interest.

Acknowledgment

References

(1)   Mutoh, K.; Miyashita, N.; Arai, K.; Abe, J. *J. Am. Chem. Soc.* **2019**, *141*, 5650.

(2)   Yamaguchi, T.; Hatano, S.; Abe, J. *J. Phys. Chem. A* **2014**, *118*, 134.

(3)   Oda, K.; Hiroto, S.; Shinokubo, H. *J. Mat. Chem. C* **2017**, *5*, 5310.

(4)   Nagura, K.; Saito, S.; Yusa, H.; Yamawaki, H.; Fujihisa, H.; Sato, H.; Shimoikeda, Y.; Yamaguchi, S. *J. Am. Chem. Soc.* **2013**, *135*, 10322.

(5)   Kobashi, T.; Sakamaki, D.; Seki, S. *Angew. Chem. Int. Ed.* **2016**, *55*, 8634.

(6)   Wang, D.; Capel Ferrón, C.; Li, J.; Gámez-Valenzuela, S.; Ponce Ortiz, R.; López Navarrete, J. T.; Hernández Jolín, V.; Yang, X.; Peña Álvarez, M.; García Baonza, V.; Hartl, F.; Ruiz Delgado, M. C.; Li, H. *Chem. Eur. J.* **2017**, *23*, 13776.

(7)   Badía-Domínguez, I.; Pérez-Guardiola, A.; Sancho-García, J. C.; López Navarrete, J. T.; Hernández Jolín, V.; Li, H.; Sakamaki, D.; Seki, S.; Ruiz Delgado, M. C. *ACS Omega* **2019**, *4*, 4761.

(8)   Zafra, J. L.; Qiu, L.; Yanai, N.; Mori, T.; Nakano, M.; Alvarez, M. P.; Navarrete, J. T. L.; Gómez-García, C. J.; Kertesz, M.; Takimiya, K.; Casado, J. *Angew. Chem. Int. Ed.* **2016**, *55*, 14563.

(9)   Yokoi, H.; Hiroto, S.; Shinokubo, H. *J. Am. Chem. Soc.* **2018**, *140*, 4649.

(10)   Yuan, L.; Han, Y.; Tao, T.; Phan, H.; Chi, C. *Angew. Chem. Int. Ed.* **2018**, *57*, 9023.

(11)   Adinarayana, B.; Shimizu, D.; Furukawa, K.; Osuka, A. *Chem. Sci.* **2019**, *10*, 6007.

(12)   Chen, X.; Wang, X.; Zhou, Z.; Sui, Y.; Sui, Y.; Ma, J.; Wang, X.; Power, P. *Angew. Chem. Int. Ed.* **2013**, *52*, 589.

(13)   Beaudoin, D.; Levasseur-Grenon, O.; Maris, T.; Wuest, J. D. *Angew. Chem. Int. Ed.* **2016**, *55*, 894.

(14)   Moshniaha, L.; Żyła-Karwowska, M.; Chmielewski, P. J.; Lis, T.; Cybińska, J.; Gońka, E.; Oschwald, J.; Drewello, T.; Rivero, S. M.; Casado, J.; Stępień, M. *J. Am. Chem. Soc.* **2020**, *142*, 3626.

(15)   Zhang, R.; Peterson, J. P.; Fischer, L. J.; Ellern, A.; Winter, A. H. *J. Am. Chem. Soc.* **2018**, *140*, 14308.

(16)   Rowan, S. J.; Cantrill, S. J.; Cousins, G. R. L.; Sanders, J. K. M.; Stoddart, J. F. *Angew. Chem. Int. Ed.* **2002**, *41*, 898.

(17)   Lehn, J.-M. *Chem. Soc. Rev.* **2007**, *36*, 151.

(18)   Sakamaki, D.; Ghosh, S.; Seki, S. *Mat. Chem. Front.* **2019**, *3*, 2270.

(19)   Alcón, I.; Viñes, F.; Moreira, I. d. P. R.; Bromley, S. T. *Nature Comm.* **2017**, *8*, 1957.

(20)   Geraskina, M. R.; Buck, A. T.; Winter, A. H. *J. Org. Chem.* **2014**, *79*, 7723.

(21)   Juetten, M. J.; Buck, A. T.; Winter, A. H. *Chem. Comm.* **2015**, *51*, 5516.

(22)   Jin, Y.; Yu, C.; Denman, R. J.; Zhang, W. *Chem. Soc. Rev.* **2013**, *42*, 6634.

(23)   Kobashi, T.; Sakamaki, D.; Seki, S. *Angew. Chem. Int. Ed.* **2016**, *128*, 8776.

(24)   Adinarayana, B.; Kato, K.; Shimizu, D.; Tanaka, T.; Furukawa, K.; Osuka, A. *Angew. Chem. Int. Ed.* **2020**, *132*, 4350.

(25)   Okino, K.; Sakamaki, D.; Seki, S. *ACS Materials Letters* **2019**, *1*, 25.

19

Accepted Manuscript

(26)   Okino, K.; Hira, S.; Inoue, Y.; Sakamaki, D.; Seki, S. *Angew. Chem. Int. Ed.* **2017**, *56*, 16597.

(27)   Peterson, J. P.; Ellern, A.; Winter, A. H. *J. Am. Chem. Soc.* **2020**, *142*, 5304.

(28)   Peterson, J. P.; Winter, A. H. *Org. Lett.* **2020**, *22*, 6072.

(29)   Zhao, H.; Jiang, L.; Dong, H.; Li, H.; Hu, W.; Ong, B. S. *ChemPhysChem* **2009**, *10*, 2345.

(30)   Ting, H.-C.; Chen, Y.-M.; You, H.-W.; Hung, W.-Y.; Lin, S.-H.; Chaskar, A.; Chou, S.-H.; Chi, Y.; Liu, R.-H.; Wong, K.-T. *J. Mat. Chem.* **2012**, *22*, 8399.

(31)   Jia, W.-b.; Wang, H.-w.; Yang, L.-m.; Lu, H.-b.; Kong, L.; Tian, Y.-p.; Tao, X.-t.; Yang, J.-x. *J. Mat. Chem. C* **2013**, *1*, 7092.

(32)   Boudreault, P.-L. T.; Virkar, A. A.; Bao, Z.; Leclerc, M. *Org. Electron.* **2010**, *11*, 1649.

(33)   Chen, S.; Wei, J.; Wang, K.; Wang, C.; Chen, D.; Liu, Y.; Wang, Y. *J. Mat. Chem. C* **2013**, *1*, 6594.

(34)   Reig, M.; Puigdollers, J.; Velasco, D. *J. Mat. Chem. C* **2015**, *3*, 506.

(35)   Khetubol, A.; Van Snick, S.; Clark, M. L.; Fron, E.; Coutiño-González, E.; Cloet, A.; Kennes, K.; Firdaus, Y.; Vlasselaer, M.; Leen, V.; Dehaen, W.; Van der Auweraer, M. *Photochem. Photobiol.* **2015**, *91*, 637.

(36)   Janosik, T.; Rannug, A.; Rannug, U.; Wahlström, N.; Slätt, J.; Bergman, J. *Chem. Rev.* **2018**, *118*, 9058.

(37)   Nakano, M.; Kishi, R.; Ohta, S.; Takahashi, H.; Kubo, T.; Kamada, K.; Ohta, K.; Botek, E.; Champagne, B. *Phys. Rev. Lett.* **2007**, *99*, 033001.

(38)   Van Snick, S.; Dehaen, W. *Org. Biomol. Chem.* **2012**, *10*, 79.

(39)   Irgashev, R. A.; Teslenko, A. Y.; Zhilina, E. F.; Schepochkin, A. V.; El'tsov, O. S.; Rusinov, G. L.; Charushin, V. N. *Tetrahedron* **2014**, *70*, 4685.

(40)   Vlasselaer, M.; Dehaen, W. *Molecules (Basel, Switzerland)* **2016**, *21*, 785.

(41)   Irgashev, R. A.; Kazin, N. A.; Rusinov, G. L.; Charushin, V. N. *Tetrahedron Lett.* **2017**, *58*, 3139.

(42)   Luo, D.; Lee, S.; Zheng, B.; Sun, Z.; Zeng, W.; Huang, K.-W.; Furukawa, K.; Kim, D.; Webster, R. D.; Wu, J. *Chem. Sci.* **2014**, *5*, 4944.

(43)   Yudina, L. N.; Preobrazhenskaya, M. N.; Korolev, A. M. *Chem. Heterocycl. Comp.* **2000**, *36*, 1112.

(44)   Streckaite, S.; Karpicz, R.; Gruodis, A.; Dehaen, W.; Van Snick, S.; Kirkus, M.; Grigalevicius, S.; Grazulevicius, J. V.; Gulbinas, V. *Dyes Pigm.* **2016**, *133*, 120.

(45)   Simokaitiene, J.; Stanislovaityte, E.; Grazulevicius, J. V.; Jankauskas, V.; Gu, R.; Dehaen, W.; Hung, Y.-C.; Hsu, C.-P. *J. Org. Chem.* **2012**, *77*, 4924.

(46)   Shi, H.; Yuan, J.; Dong, X.; Cheng, F. *Spectrochim. Acta A Mol. Biomol. Spectrosc.* **2014**, *133*, 501.

(47)   Shi, H.-p.; Dai, J.-x.; Wu, X.-h.; Shi, L.-w.; Yuan, J.-d.; Fang, L.; Miao, Y.-q.; Du, X.-g.; Wang, H.; Dong, C. *Org. Electron.* **2013**, *14*, 868.

(48)   Bintinger, J.; Yang, S.; Fruhmann, P.; Holzer, B.; Stöger, B.; Svirkova, A.; Marchetti-Deschmann, M.; Horkel, E.; Hametner, C.; Fröhlich, J.; Kymissis, I.; Mikula, H. *Synth. Met.* **2017**, *228*, 9.

(49)   Jiménez, V. A.; Gavín, J. A.; Alderete, J. B. *Struct. Chem.* **2012**, *23*, 123.

(50)   van Dongen, M. A.; Orr, B. G.; Banaszak Holl, M. M. *T J. Phys. Chem. B* **2014**, *118*, 7195.

(51)   Fu, X.; Zhao, D. *Org. Lett.* **2015**, *17*, 5694.

(52)   Wang, D.; Ivanov, M. V.; Kokkin, D.; Loman, J.; Cai, J.-Z.; Reid, S. A.; Rathore, R. *Angew. Chem. Int. Ed.* **2018**, *130*, 8321.

(53)   Ferrón, C. C.; Capdevila-Cortada, M.; Balster, R.; Hartl, F.; Niu, W.; He, M.; Novoa, J. J.; López Navarrete, J. T.; Hernández, V.; Ruiz Delgado, M. C. *Chem. Eur. J.* **2014**, *20*, 10351.

(54)   González-Cano, R. C.; Di Motta, S.; Zhu, X.; López Navarrete, J. T.; Tsuji, H.; Nakamura, E.; Negri, F.; Casado, J. *J. Phys. Chem.* **2017**, *121, 23141.*

20

(55)   González Cano, R. C.; Herrera, H.; Segura, J. L.; López Navarrete, J. T.; Ruiz Delgado, M. C.; Casado, J. *ChemPhysChem* **2012**, *13*, 3893.

(56)   Bauer, C. A.; Hansen, A.; Grimme, S. *Chem. Eur. J.* **2017**, *23*, 6150.

(57)   Stanger, A. *J. Org. Chem.* **2006**, *71*, 883.

(58)   Mosca, S.; Milani, A.; Peña-Álvarez, M.; Yamaguchi, S.; Hernández, V.; Ruiz Delgado, M. C.; Castiglioni, C. *J. Phys. Chem. C* **2018**, *122*, 17537.

(59)   Yang, K.; Zhang, X.; Harbuzaru, A.; Wang, L.; Wang, Y.; Koh, C.; Guo, H.; Shi, Y.; Chen, J.; Sun, H.; Feng, K.; Ruiz Delgado, M. C.; Woo, H. Y.; Ortiz, R. P.; Guo, X. *J. Am. Chem. Soc.* **2020**, *142*, 4329.

(60)   Zeng, Z.; Lee, S.; Zafra, J. L.; Ishida, M.; Zhu, X.; Sun, Z.; Ni, Y.; Webster, R. D.; Li, R.-W.; López Navarrete, J. T.; Chi, C.; Ding, J.; Casado, J.; Kim, D.; Wu, J. *Angew. Chem. Int. Ed.* **2013**, *52*, 8561.

(61)   Baonza, V. G.; Taravillo, M.; Arencibia, A.; Cáceres, M.; Núñez, J. *J. Raman Spectrosc. y* **2003**, *34*, 264.

(62)   Alvarez, M. P.; Burrezo, P. M.; Kertesz, M.; Iwamoto, T.; Yamago, S.; Xia, J.; Jasti, R.; Navarrete, J. T. L.; Taravillo, M.; Baonza, V. G.; Casado, J. *Angew. Chem. Int. Ed.* **2014**, *53*, 7033.

(63)   Peña-Alvarez, M.; Qiu, L.; Taravillo, M.; Baonza, V. G.; Delgado, M. C. R.; Yamago, S.; Jasti, R.; Navarrete, J. T. L.; Casado, J.; Kertesz, M. *Phys. Chem. Chem. Phys.* **2016**, *18*, 11683.

(64)   Qiu, L.; Peña-Alvarez, M.; Baonza, V. G.; Taravillo, M.; Casado, J.; Kertesz, M. *ChemPhysChem* **2018**, *19*, 1903.

(65)   Qiu, L.; Peña-Alvarez, M.; Taravillo, M.; Evans, P. J.; Darzi, E. R.; Jasti, R.; Burrezo, P. M.; López Navarrete, J. T.; Baonza, V. G.; Casado, J.; Kertesz, M. *Chem. Eur. J.* **2017**, *23*, 16593.